Journal of Molecular Graphics and Modelling 38 (2012) 248–255

Contents lists available at SciVerse ScienceDirect

Journal of Molecular Graphics and Modelling

journal homepage: www.elsevier.com/locate/JMGM

Computational study: How redox affect the nonlinear optical properties of donor substituted heteroleptic bis-tridentate Ru(II) complexes?

Xiu-Xin Sun, Na-Na Ma, Xiao-Juan Li, Shi-Ling Sun, Hai-Ming Xie*, Yong-Qing Qiu**

Institute of Functional Material Chemistry, Faculty of Chemistry, Northeast Normal University, Changchun 130024, PR China

ARTICLE INFO

Article history:
Accepted 2 July 2012
Available online 18 August 2012

Keywords:
Ru(II) complex
Donor substituent
Deprotonation
Redox
NLO property

ABSTRACT

Donor substituted heteroleptic bis-tridentate Ru(II) complexes with different deprotonated forms exhibit larger alterations of the first hyperpolarizabilities in oxidized process and are promising to become redox-switchable nonlinear optical (NLO) molecular materials. For systems with diprotonated form, the β_{vec} value of the two-electron-oxidized system $\mathbf{1}^{3+}$ is 5.3 and 178.6 times as large as those of the reduced parent **3** and the one-electron-oxidized system $\mathbf{3}^{+}$ according to the DFT–FF results. For systems with mono-protonated form, the oxidization of the deprotonated benzimidazole anion is more helpful to enhance the β_{vec} value because of the increasing β_x component. For systems with fully deprotonated form, the largest ratio of $|\beta_{vec}(\mathbf{(1'')^{+}})/\beta_{vec}(\mathbf{1''})|$ of the system without substituent is about 13.2 due to the dominant off-diagonal tensor β_{zxx}. And the time-dependent density functional theory (TDDFT) results indicate that the charge transfer transition of the first excited state displays an indispensable role for larger off-diagonal tensor. Finally, the calculated frequency-dependent β results exhibit a small dispersion effect at the low-frequency region.

1. Introduction

Switchable nonlinear optical (NLO) molecular materials have attracted considerable attention because of their novel and interesting applications in optoelectronic technologies [1,2]. Generally speaking, the NLO behavior could be switched by reversibly modifying the capacity of the donor/acceptor and the nature of the π-conjugated bridge. Among them, the more appealing scheme is based on lowering the donor/acceptor capacity of a typical donor–acceptor (D–A) species by oxidation/reduction or protonation/deprotonation [3–6]. In order to obtain an effective switching, the molecule must be stable in two (or more) states that offer different NLO responses.

Organotransition metal complexes have always been chosen as the candidates of multifunctional NLO materials due to their excellent electrochemical and optical (linear and nonlinear) properties [2,7–9]. Especially, metal-based redox, which reversibly switches different types of NLO phenomena, is becoming the promise in switchable-NLO field for its easy acquirement [1–4]. Coe et al. [10,11] have reported a range of V-shaped metal-based chromophores with reversible $Ru^{III/II}$ waves. Results suggest that those complexes possess the potential as redox-switchable NLO chromophores because of their large first hyperpolarizabilities β that governs quadratic NLO response at the molecular level. Most intriguing, these metallochromophores show two-dimensional (2D) NLO character because of the dominant off-diagonal β_{zyy} tensor. Compared to traditional 1D species, multidimensional NLO chromophores, which show more than one charge transfer (CT) directions, could offer better nonlinearity/transparency trade-off. Therefore, multidimensional NLO molecules have been considered as candidates for optimization of NLO responses [10–15].

Tridentate ligand 2,6-bis(benzimidazole-2-yl)pyridine (LH_2) and its derivatives have been coordinated to transition metals for structure and property investigations [16–21]. This kind of ligands is so attractive that they can offer a combination of moderate π-acceptor pyridine nitrogen and π-donor imidazole nitrogen. Moreover, the presence of one or more dissociable N—H proton makes it possible to tune the spectroscopic and redox properties by deprotonation. Ruthenium complexes with the tridentate ligand LH_2 have been studied on their photophysical and electrochemical properties [20–23]. Results show that both the absorption spectra and the redox potentials are strongly pH-dependent in consequence of the ligand based completely reversible protonation or deprotonation processes. According to the work taken by Mondal et al. [22], the approximate numerical dependency of deprotonation and redox process of a set of Ru monoterpyridine (tpy) complexes are summarized and shown in Scheme 1. Among them, both the diprotonated and fully deprotonated forms have been isolated as solid crystals and demonstrated to show excellent electrochemical behaviors. Although the cyclic voltammogram

* Corresponding author.
** Corresponding author. Fax: +86 431 85098768.
E-mail addresses: xiehm136@nenu.edu.cn (H.-M. Xie), qiuyq466@nenu.edu.cn (Y.-Q. Qiu).

1093-3263/$ – see front matter © 2012 Elsevier Inc. All rights reserved.
http://dx.doi.org/10.1016/j.jmgm.2012.07.001

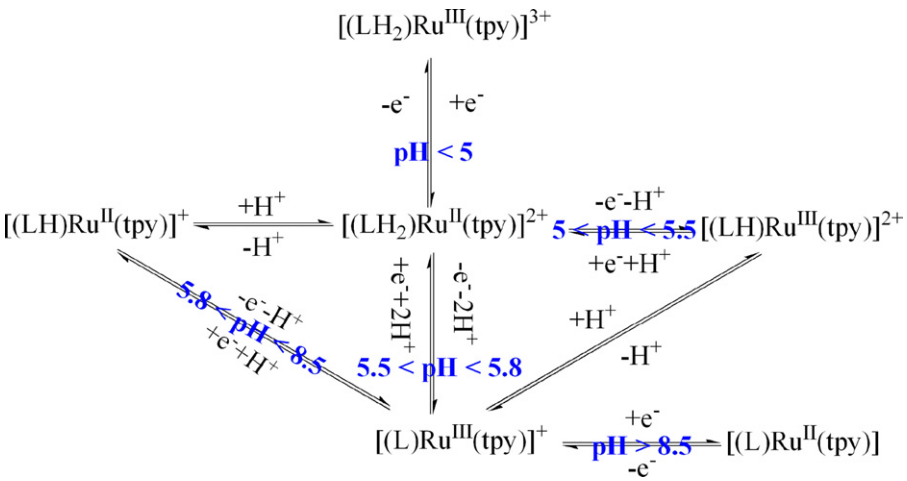

Scheme 1. pH dependence of electron transfer, proton transfer and proton coupled electron transfer processes in acetonitrile:water (1:4, v/v). From Ref. [22].

involving the mono-deprotonated forms has not been apparently involved, pH dependent absorption spectral changes do clearly indicate the existence of mono-deprotonated intermediate.

Prior to this work, we studied the NLO properties on a family of complexes $[(LH_2)Ru^{II}(tpy\text{-}X)]^{2+}$ with different electron-donating and electron-withdrawing groups together with their deprotonated forms [24]. We found that the introduced group X acts as an donor in the CT process, therefore the addition of electron-donating moiety is good for larger CT and larger NLO coefficient. Tetrathiafulvalene (TTF) unit is not only an efficient π-electron donor but also an excellent redox-active center due to the possibility of reversible stepwise oxidation forming stable radical cation and dication species ($TTF \leftrightarrow TTF^{\bullet+} \leftrightarrow TTF^{2+}$) [25]. Redox-switchable NLO properties on organic and organometallic TTF systems have been studied both experimentally and theoretically, and the static first hyperpolarizability β substantially is changed by the oxidized TTF species [15,26,27]. Thus, we further study the relationship between redox states and second-order NLO responses for complexes $[(LH_2)Ru^{II}(tpy\text{-}X)]^{2+}$ couple with deprotonation, where X points to H (species **1**), Ph-NMe_2 (species **2**) and monopyrrolo-TTF (species **3**) (Fig. 1). There are two reasons that we choose the monopyrrolo-TTF moiety instead of simple TTF unit as substituent. One is that the basic skeleton of the substituted tpy ligand is kept the same and the branch is along the coordinate axis. The other is that this kind of organics has been synthesized and the cyclic voltammetry shows two pairs of reversible redox waves [25,28,29].

2. Computational details

All calculations in this work were performed using the Gaussian 09W program package [30]. The structures of all complexes were optimized at the (U)B3LYP/6-31G* level (LANL2DZ basis set for Ru atom) without symmetry constraint. And vibrational frequency calculations were carried out to verify that the obtained structures are local minima on the potential energy surface.

The static first hyperpolarizability tensors of all complexes were calculated by finite field (FF) method with a field frequency of 0.0010 a.u. The FF method is broadly applied to investigate the NLO response as this methodology can be used in concert with the electronic structure method to compute β [31]. In the present paper,

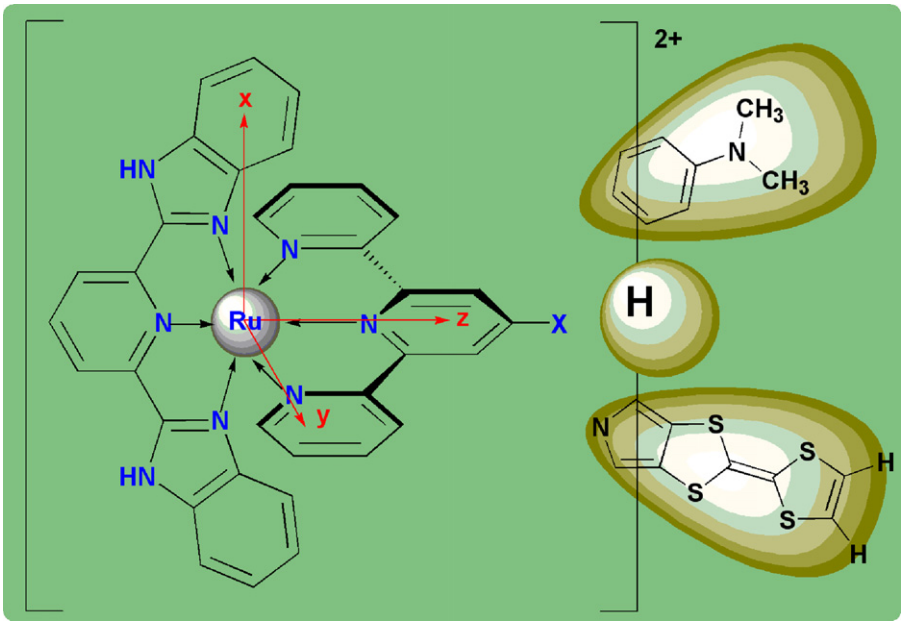

Fig. 1. Structural formulas of complexes coupled with substituents.

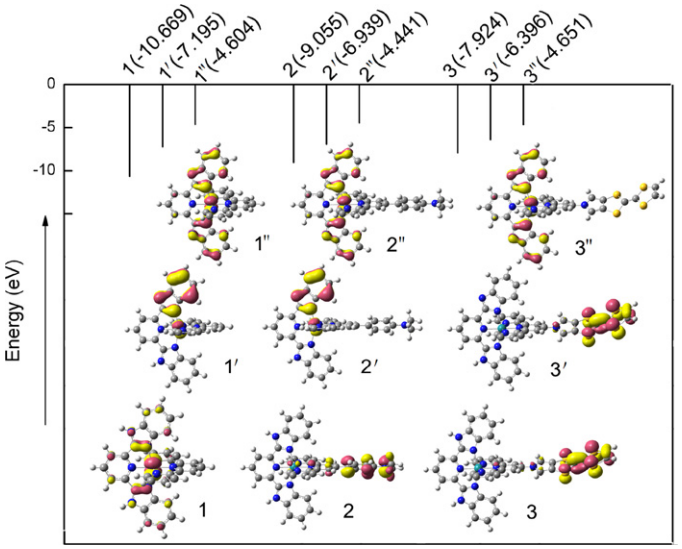

Fig. 2. The highest occupied molecular orbitals (HOMOs) and the corresponding energies (eV) for the reduced parents.

CAM-B3LYP/6-31G* has been employed to evaluate qualitatively the optical nonlinearity of the studied complexes. Frequency-dependent β values were also calculated by coupled-perturbed DFT method to estimate the dispersion effect. For dipolar molecules, the first hyperpolarizability is generally related to the β_{vec} value, which is the vector component of β along the dipole moment direction, given by Eq. (1) [31]:

$$\beta_{vec} = \sum_{i=1}^{3} \frac{\mu_i \beta_i}{|\mu|} \quad (1)$$

Here μ is the ground-state molecular dipole moment and β_i is defined as (Eq. (2)):

$$\beta_i = \beta_{iii} + \frac{1}{3}\sum_{i \neq j}[(\beta_{ijj} + \beta_{jij} + \beta_{jji})] \quad i,j = x, y, z \quad (2)$$

To further understand the electron structures of the studied complexes, UV–vis absorption spectra were calculated by time-dependent density functional theory (TDDFT) method and Density-of-States (DOS) were analyzed using the AOMix program [32].

3. Results and discussion

Before all properties being discussed, it is necessary to define the three species. According to the different protonation, each species is categorized into three systems, for example: system **1** (diprotonated), system **1′** (mono-deprotonated), and system **1″** (fully deprotonated). Considering the oxidation, every system has its oxidized form while the system itself acts as the reduced parent.

3.1. Redox properties

It is well-known that the redox property of a molecule is closely related to the nature of the frontier molecular orbital (FMO). Fig. 2 shows the highest occupied molecular orbitals (HOMOs) for all the reduced parents. An analysis indicates that, for systems with diprotonated form (systems **1**–**3**), the HOMOs are obviously affected by the substituents. With the increasing electron-donating ability ($H < NMe_2 < TTF$), the distribution of electron density shifts from the metal ion to the substituent and is almost entirely located on the TTF unit in system **3**, which suggests that the oxidized center changes into ligand instead of the center metal. As for the mono-deprotonated and fully deprotonated systems (except system **3′**), the HOMOs have similar patterns: both the metal ion and the deprotonated benzimidazole anion play major contribution to the HOMOs and could be the oxidized centers. While for system **3′**, the HOMO is localized on the TTF unit and thus the TTF unit will be the oxidized center of system **3′**. Finally, the distributions of spin densities for all the corresponding oxidized forms also clearly support our idea about the oxidized center (see Fig. S1 in Supporting information). Due to the excellent redox property of the TTF moiety and good thermodynamic stability of its oxidized states, not only the one-electron-oxidized systems, $\mathbf{3^+}$/$\mathbf{(3')^+}$, but also two-electron-oxidized systems, $^1\mathbf{3^{2+}}$/$^3\mathbf{3^{2+}}$ and $^1\mathbf{(3')^{2+}}$/$^3\mathbf{(3')^{2+}}$ (two possible spin states: singlet state and triplet state) have been concerned and discussed. The following frequency calculations indicate that each of the oxidized geometries is a minimum (no imaginary frequency) on the potential energy surface, and their spin density plots (Fig. S1) display that the two-electron-oxidized centers locate on the TTF moiety.

Table 1
Ground-state dipole moments (a.u.) and static first hyperpolarizabilities ($\times 10^{-30}$ esu) for the diprotonated systems, $[(LH_2)Ru^{II}(tpy\text{-}X)]^{2+}$, with their oxidized forms (CAM-B3LYP/6-31g* (LANL2DZ basis set on Ru atom)).

System	μ_z	β_{zzz}	β_z	β_{vec}
1	−1.256	−5.17	−16.00	16.00
$\mathbf{1^+}$	−1.481	−5.56	−7.23	7.23
2	−2.624	−180.10	−186.16	186.17
$\mathbf{2^+}$	4.606	664.91	653.30	653.35
3	−8.514	−573.31	−581.10	580.66
$\mathbf{3^+}$	1.478	19.36	17.18	17.18
$^1\mathbf{3^{2+}}$	8.247	3060.58	3068.47	3068.83
$^3\mathbf{3^{2+}}$	−2.126	−158.24	−136.74	136.75

3.2. Static second-order NLO properties

3.2.1. Static second-order NLO switching for systems with diprotonated form

DFT–FF calculations indicate that the static first hyperpolarizabilities for the systems with diprotonated form mainly derive from the β_z component along the dominant dipole moment direction μ_z, so that the numerical values of β_{vec} and β_z are approximately equal as shown in Table 1. An analysis of Table 1 reveals that, for the reduced parents, the stronger donor capability of the substituent, the larger first hyperpolarizability. The β_{vec} value of 580.66×10^{-30} esu for system **3** with TTF donor is 36.3 times as large as that for system **1**, which further demonstrates the conclusion obtained in our previous work [24]. As for the oxidized forms, the oxidization of system **1** without substituent cannot effectively enhance the second-order NLO response. The calculated β_{vec} value of system $\mathbf{1^+}$ is halved compared with that of its reduced parent **1**. For the species with donor substituents, however, the second-order NLO responses are significantly enhanced after oxidization. The calculated β_{vec} value of system $\mathbf{2^+}$ is 3.5 times as large as that of the reduced parent **2**. Although the β_{vec} value of 17.18×10^{-30} esu for the one-electron-oxidized system $\mathbf{3^+}$ is 0.03 times as small as that of the reduced parent **3**, the β_{vec} value of two-electron-oxidized systems $^1\mathbf{3^{2+}}$ increases to 3068.83×10^{-30} esu which is 5.3 and 178.6 times as large as those of the parent **3** and the system $\mathbf{3^+}$. These indicate that the ejection of electrons has a more significant effect on the second-order NLO response of the system **3** with TTF unit and the system **3** is more promising to become excellent redox-switchable NLO molecular material.

In order to get more insights into the second-order NLO responses of species **3**, we have performed the TDDFT computations and the crucial excited states are summarized in Table 2. To

Table 2
TDDFT results for system **3** and its oxidized forms (CAM-B3LYP/6-31g* (LANL2DZ basis set on Ru atom) and L = LH_2, L′ = tpy-X).

System	ΔE_{ge} (eV)	f_{os}	Major contributions	Assignment
	2.02	0.3500	HOMO → LUMO + 2 (95%)	L′MCT/IL′CT
3	3.34	0.2856	HOMO → LUMO + 4 (60%) HOMO → LUMO + 6 (15%)	ML′CT/IL′CT
	3.98	0.4501	HOMO − 7 → LUMO (50%) HOMO − 6 → LUMO + 3 (21%)	ML′CT ILCT
	2.28	0.2239	βHOMO − 8 → βLUMO (54%) βHOMO − 1 → βLUMO (20%)	ML′CT
3^{+}	3.21	0.2991	αHOMO − 4 → αLUMO (27%) βHOMO − 1 → βLUMO + 1 (22%)	ML′CT/IL′CT
	3.47	0.2848	αHOMO → αLUMO + 5 (18%) αHOMO → αLUMO + 6 (29%)	ML′CT/IL′CT ILCT
	3.99	0.6100	αHOMO − 3 → αLUMO + 2 (34%) βHOMO − 3 → βLUMO + 3 (34%)	ILCT
	1.17	0.2331	HOMO − 4 → LUMO (99%)	ML′CT/IL′CT
$^{1}\mathbf{3}^{2+}$	2.75	0.7014	HOMO − 14 → LUMO (64%) HOMO − 11 → LUMO (19%)	ML′CT/IL′CT
	4.02	0.5849	HOMO − 1 → LUMO + 6 (67%)	ILCT
	2.53	0.2600	αHOMO → αLUMO (56%)	L′MCT/IL′CT
$^{3}\mathbf{3}^{2+}$	3.40	0.3244	αHOMO → αLUMO + 11 (19%) βHOMO − 7 → βLUMO + 1 (11%) βHOMO − 1 → βLUMO + 3 (14%)	ML′CT/IL′CT
	3.61	0.3951	αHOMO − 2 → αLUMO + 1 (28%) βHOMO − 2 → βLUMO + 2 (35%)	L′MCT ILCT

clearly observe the electron transitions, we also describe the electron density difference maps (EDDM) as shown in Fig. 3, the blue represents where the electrons are coming from and the purple represents where the electrons are going. Obviously, the electron transitions of the crucial excited states are divided into two categories. One is the ILCT transition along the *x*-axis, which leads to the small β_x component of diprotonated systems due to the opposite CT direction from the benzimidazole at each end of LH_2 ligand to the central pyridine. The other is the CT transition located at the metal and tpy-X ligand along the *z*-axis, which dominate the NLO responses of the studied systems. It is apparent that the oxidation alters the characteristic of CT from *z*-axis including the degree and the direction. The electron transitions of the reduced parent **3** are viewed as IL′CT and L′MCT along the negative *z*-axis, and thus the TTF unit acts as donor while the central metal and the tpy moiety act as acceptors. The electron transitions of the system **3**$^{+}$ are mainly attributed to ML′CT from Ru to tpy group along the positive *z*-axis and IL′CT from TTF unit to tpy group along the negative *z*-axis, and the opposite CT direction will significantly reduce its β value. The CT characteristics of the system $^{3}\mathbf{3}^{2+}$ are similar to those of the reduced parent and attributed to the IL′CT and L′MCT along the negative *z*-axis. Notably, there is also an opposing ML′CT transition in system $^{3}\mathbf{3}^{2+}$ and the reduced parent **3**, which has a negative effect on their β values. As for the system $^{1}\mathbf{3}^{2+}$, the CT characteristics are different from the others and belong to ML′CT and IL′CT along the positive *z*-axis, and such CT transitions lead to the largest β value. That is, large NLO responses can be obtained when the metal or the tpy moiety turns to donor while the TTF unit turns to acceptor.

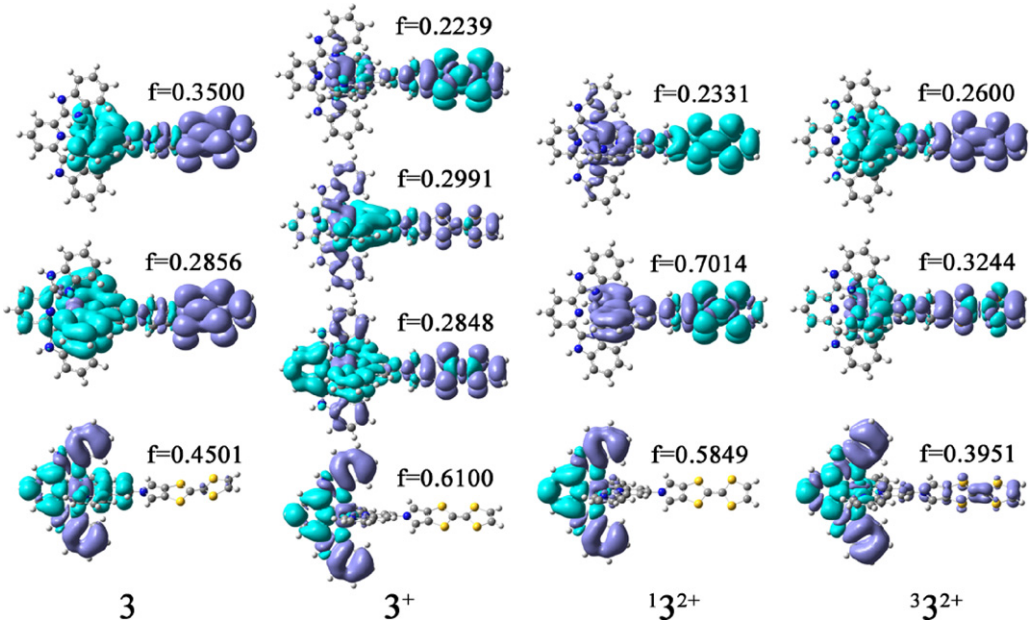

Fig. 3. Electron density difference maps (EDDM) of the crucial excited states for the species **3**. The electrons increased are visualized by blue regions whereas the electrons decreased are purple. (For interpretation of the references to color in this figure legend, the reader is referred to the web version of the article.)

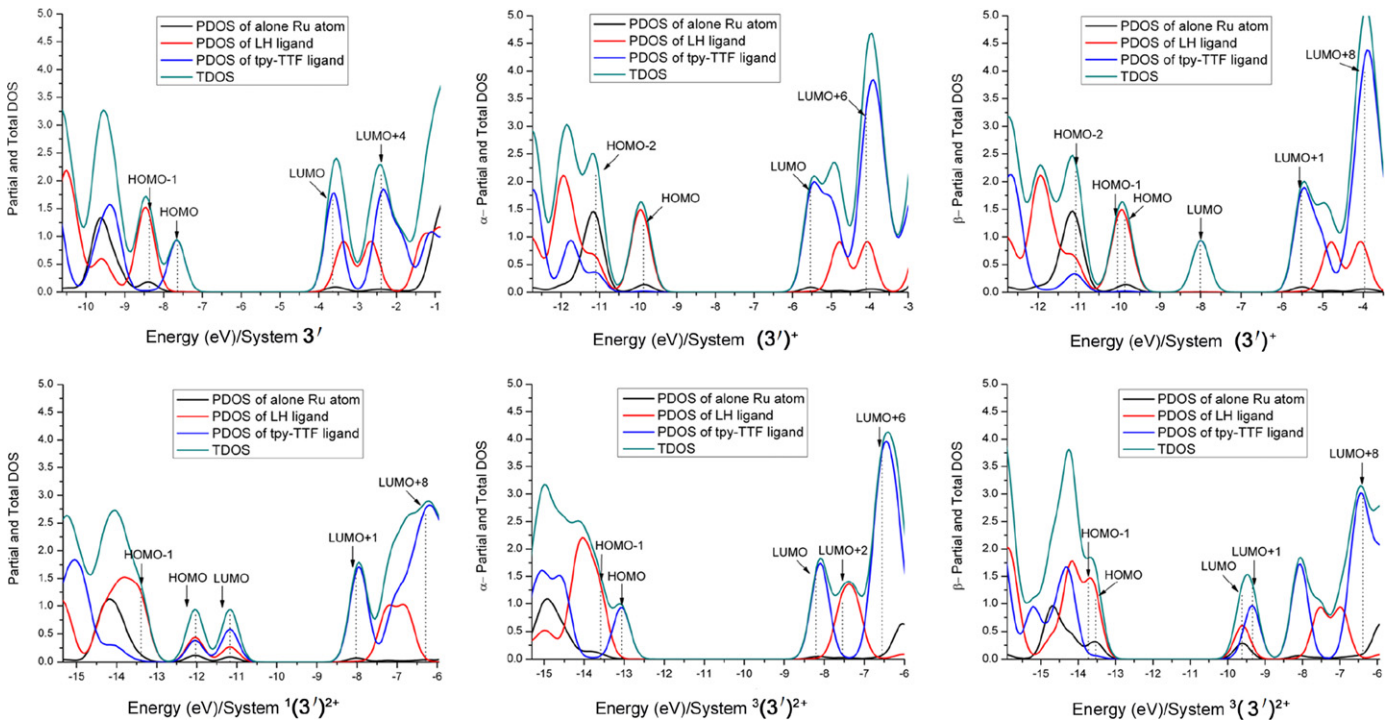

Fig. 4. Partial and total Density-of-States (PDOS and TDOS) for all the mono-deprotonated species **3**.

3.2.2. *Static second-order NLO switching for systems with mono-deprotonated form*

As described in our previous work, the single proton abstraction leads to a large change of the dipole moment component μ_x and a remarkable increase in the β_x value due to the asymmetric electronic distribution along the *x*-axis [24]. The calculated results for all the mono-deprotonated systems and their oxidized forms are listed in Table 3. The character η refers to the ratio β_x/β_z, which means the relative contribution of the *x*-axis and *z*-axis to the NLO properties of complexes. It is clearly noticed that the absolute values of the ratio, $|\eta|$, are greatly enhanced in the oxidized processes: the $|\eta|$ value of **(1′)⁺** increases to 8.47 from 2.03 of **1′**, the $|\eta|$ value of the **(2′)⁺** increases to 1.80 from 0.23 of **2′**, and the $|\eta|$ values of the two-electron-oxidized systems **^{1}(3′)$^{2+}$** and **^{3}(3′)$^{2+}$** increase to 0.75 and 1.37 from 0.11 of **3′**, respectively. This points out that the oxidized process further increases the contribution from the *x*-polarized transition with respect to mono-deprotonated parents. Furthermore, we could also see that the $|\eta|$ value of system **^{1}(3′)$^{2+}$** is slightly larger than 0.5. It indicates that two intersecting CT transitions are observed due to both the *x*-polarization and *z*-polarization of the dipole, which codetermines the NLO property.

Unlike the systems with diprotonated form, the β_{vec} values of the systems with mono-deprotonated form are no longer approximately equal to the β_z values due to the *x*-polarized dipole and the corresponding *x*-polarized transition. The one-electron-oxidized systems **(1′)⁺** and **(2′)⁺** show significantly large β_{vec} values of 178.62×10^{-30} and 336.39×10^{-30} esu, respectively, which are 9.4 and 90.2 times as large as those of their reduced parents. However, the β_{vec} value of 261.19×10^{-30} esu for system **(3′)⁺** is only 1.9 times as large as that of its reduced parent **3′**. According to the discussion in Section 3.1, the oxidized center of **3′** is still located on the moiety TTF instead of the deprotonated benzimidazole anion. Thus there is a noticeable change on the β_z (including the absolute value and the sign) rather than β_x in the oxidized process of **3′**, and finally a smaller increase occurs on the β_{vec} value of **(3′)⁺**. As for the two-electron-oxidized systems **^{3}(3′)$^{2+}$** and **^{1}(3′)$^{2+}$**, the β_{vec} values do not show significant changes although the β_x components increase obviously. Therefore, it is not advisable to enhance the β_{vec} value by introducing stronger donor in oxidized process for the mono-deprotonated systems.

Because of the multi-dimensional NLO characters of the mono-deprotonated systems, various electronic CT excited states will contribute to the NLO responses and the contributions of various excited states to the β_i ($i = x$ and z) component will be different. To further observe these differences, we will take the species **3′** as an example to study the electronic structures by the analysis of the partial Density-of-States (PDOS) and total Density-of-States (TDOS) from orbital HOMO − 10 to orbital LUMO+10. As plotted in Fig. 4, in the parent system **3′** the tpy-TTF unit plays a complete contribution in the formation of its HOMO while in its oxidized systems the contribution decreases largely. This point demonstrates that the TTF moiety is the system's oxidized center, and this is well in agreement with the conclusion obtained in Section 3.1. Analyzing the PDOS of ligands in Fig. 4 together with the EDDM in Fig. S2, in the one-electron-oxidized system **(3′)⁺**, the tpy-TTF ligand has the largest CT contribution and it is mainly attributed to the *z*-axis transition, and thus the β_z value increases. Notably, the tpy-TTF unit acts as an acceptor in system **(3′)⁺** instead of as a donor, which inevitably alters the sign of β_z. Considering the two-electron-oxidized systems, the CT contribution from the LH

Table 3
Ground-state dipole moments (a.u.) and static first hyperpolarizabilities ($\times 10^{-30}$ esu) for the mono-deprotonated systems, $[(LH)Ru^{II}(tpy\text{-}X)]^+$, with their oxidized forms (CAM-B3LYP/6-31g* (LANL2DZ basis set on Ru atom)).

System	μ_x	μ_z	β_x	β_z	β_{vec}	$\|\eta\|$
1′	−3.686	0.808	−21.79	−10.76	18.99	2.03
(1′)⁺	−1.634	0.503	−193.90	−22.91	178.62	8.47
2′	−3.699	0.977	−22.94	−101.54	−3.73	0.23
(2′)⁺	−1.935	−0.237	−317.31	−176.22	336.39	1.80
3′	−3.363	−3.570	−19.49	−174.78	140.59	0.11
(3′)⁺	−2.986	4.550	−14.75	302.71	261.19	0.05
^{1}(3′)$^{2+}$	−1.471	5.312	308.24	409.26	312.20	0.75
^{3}(3′)$^{2+}$	−1.426	3.549	76.01	−55.50	−79.84	1.37

Table 4
Ground-state dipole moments (a.u.) and static first hyperpolarizabilities ($\times 10^{-30}$ esu) for the fully deprotonated systems, [(L)Ru^{II}(tpy-X)], with their oxidized forms (CAM-B3LYP/6-31g* (LANL2DZ basis set on Ru atom)).

System	μ_z	β_x	β_z	β_{vec}	β_{zxx}	β_{zzz}
1″	2.727	−0.064	−4.52	−4.52	−10.42	−0.22
(1″)$^+$	2.571	0.53	59.74	59.74	59.09	−0.60
2″	4.702	−0.73	−41.55	−41.55	−8.99	−39.20
(2″)$^+$	3.134	−4.22	−42.22	−42.27	77.57	−123.57
3″	2.607	1.05	−62.48	−62.04	−8.86	−61.22
(3″)$^+$	−0.992	7.63	−147.83	145.32	94.28	−246.49

ligand increases compared with systems **3**′ and **(3′)$^+$** and thus larger β_x values are obtained. However, the CT contribution from ligand tpy-TTF decreases obviously, especially in the α-MO-DOS of system **^{3}(3′)$^{2+}$**. Even so, the energy gap between HOMO and LUMO greatly decreases in system **^{1}(3′)$^{2+}$**, which can be the factor leading to larger alteration on β_z value. To sum up, the CT transitions from ligands after oxidization do not effectively alter the β_{vec} values and thus the mono-deprotonated systems with TTF unit are not suitable for redox-switchable NLO materials.

3.2.3. Static second-order NLO switching for systems with fully deprotonated form

The fully deprotonated systems have similar NLO character to the diprotonated ones: the static first hyperpolarizabilities mainly derive from the β_z component along the dominant dipole moment direction μ_z as shown in Table 4. We have known that the oxidized centers of all the fully deprotonated systems are located on the deprotonated benzimidazole anion and the CT along the *x*-axis will be inevitably influenced, therefore the β_x value is also listed in Table 4 for discussion. Clearly, the β_x component increases greatly after oxidization although the contribution of the β_x component to the β_{vec} value is small. As seen from Table 4, the change of β_z is mainly caused by the change of the off-diagonal tensor β_{zxx} including the numerical value and the sign, which suggests that the oxidized process not only alters the CT degree but also adjusts the CT direction. Notably, for systems with donor substituents, the change of the sign of β_{zxx} exerts a negative influence on the increase of β_{vec} due to the principal role of β_{zzz} to β_{vec}, and thus smaller increase is observed: $|\beta_{vec}(\mathbf{(2'')^+})/\beta_{vec}(\mathbf{2''})| \approx 1.0$ and $|\beta_{vec}(\mathbf{(3'')^+})/\beta_{vec}(\mathbf{3''})| \approx 2.3$. For system **1**″, however, the ratio of $|\beta_{vec}(\mathbf{(1'')^+})/\beta_{vec}(\mathbf{1''})|$ increases to 13.2 due to the dominant role of the off-diagonal tensor β_{zxx} to β_{vec}, which reflects that the system without substituent shows the more potential as redox-switchable NLO chromophore in the fully deprotonated systems.

For the studied complexes, the *z*-polarized transition contributes to the diagonal tensor β_{zzz} and *x*-polarized transition contributes to the off-diagonal tensor β_{zxx}. In order to understand the detail of these transitions, the *z*- and *x*-polarized transition dipole moments of two crucial excited states together with the first excited state are plotted as a graph in Fig. 5 according to the TDDFT results. It can be seen that one of the two crucial excited states is attributed to *z*-polarized transition while the other is attributed to *x*-polarized transition. However, all the excited states of system **(1″)$^+$** account for the *x*-polarized transition, which can be one of the reasons leading to its larger β_{zxx}/β_{zzz}. Compared the oxidized systems with their reduced parents, the most obvious difference is the contribution from the first excited state. In oxidized systems, the *x*-polarized transition from the first excited state plays an indispensable role, resulting in larger off-diagonal tensor β_{zxx} and enhancing the NLO responses.

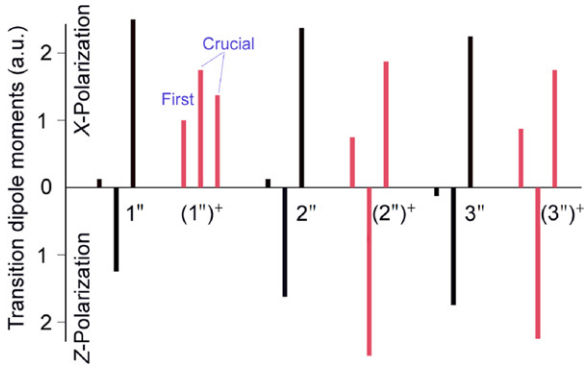

Fig. 5. Transition dipole moments of all the fully deprotonated systems with their oxidized states calculated by TDDFT method.

Table 5
The estimated frequency-dependent β_{vec} ($\times 10^{-30}$ esu) for the species **3** with diprotonated form.

System	ω (a.u.)	SHG $\beta(-2\omega; \omega, \omega)$	OR $\beta(0; \omega, -\omega)$
3	0.005	581.04	571.79
	0.01	626.05	585.83
3$^+$	0.005	17.64	17.00
	0.01	20.69	17.94
^{1}3^{2+}	0.005	2964.50	2755.57
	0.01	22,430.73	3086.54
^{3}3^{2+}	0.005	136.08	136.32
	0.01	146.46	171.21

3.3. Frequency-dependent second-order NLO properties

In order to understand the dispersion effect of second-harmonic generation (SHG) and optical rectification (OR) on the NLO responses, frequency-dependent β values were calculated by coupled-perturbed DFT method, and the same functional and basis sets with FF method were employed. Table 5 lists the calculated values $\beta(-2\omega; \omega, \omega)$, $\beta(0; \omega, -\omega)$ at $\omega = 0.005$ and 0.01 a.u. for the species **3** with diprotonated form.

As shown in Table 5, the computed frequency-dependent $\beta(-2\omega; \omega, \omega)$ and $\beta(0; \omega, -\omega)$ are approximately equal to the corresponding static β_{vec} values, except for the $\beta(-2\omega; \omega, \omega)$ at $\omega = 0.01$ a.u. of system **^{1}3^{2+}**. The results indicate that the studied complexes exhibit a small dispersion effect at the low-frequency region. It is well known that large β will be obtained at an input photon energy close to one-photon (ω) or two-photon (2ω) resonance energy [33]. For system **^{1}3^{2+}**, the transition energy of the first excited state is 0.02 a.u. (0.5499 eV as shown in Table 2) and equal to 2ω ($\omega = 0.01$ a.u.), which means that the two-photon resonance absorption leads to the sharp increase in $\beta(-2\omega; \omega, \omega)$ value at $\omega = 0.01$ a.u. ($22{,}430.73 \times 10^{-30}$ esu about 7.4 times larger than $\beta(0; 0, 0)$). Moreover, it is clear to see that the frequency-dependent β also show large alterations in the series of oxidized processes, which further suggests that the second-order NLO responses of the studied complexes can be strongly affected by oxidization.

4. Conclusions

The effect of redox on the NLO properties of heteroleptic bis-tridentate Ru(II) complexes with donor substituents in different protonated forms is theoretically investigated. Larger alterations of the first hyperpolarizabilities have been observed and the studied complexes are promising to become the excellent redox-switchable NLO molecular materials. For systems with

diprotonated form, the changes of the static first hyperpolarizabilities β_{vec} are different after oxidization due to the different oxidized center in the three species. The species **3** with stronger donor substituent have the most obvious alterations, for example, the β_{vec} value of two-electron-oxidized system $^{1}\mathbf{3}^{2+}$ increases to 3068.83×10^{-30} esu which is 5.3 and 178.6 times as large as those of the reduced parent **3** (580.66×10^{-30} esu) and the one-electron-oxidized system $\mathbf{3}^{+}$ (17.18×10^{-30} esu). TDDFT results display that the ML′CT and IL′CT transitions along the positive *z*-axis lead to the largest β_{vec} value of system $^{1}\mathbf{3}^{2+}$. For systems with mono-protonated form, the oxidization of deprotonated benzimidazole anion further increases the contribution from the *x*-polarized transition with respect to the mono-deprotonated parents: the β_{vec} values of 178.62×10^{-30} esu of system $(\mathbf{1}')^{+}$ and 336.39×10^{-30} esu of system $(\mathbf{2}')^{+}$ are 9.4 and 90.2 times as large as those of their reduced parents, respectively. For systems with fully deprotonated form, the increase of the off-diagonal tensor β_{zxx} plays a negative role in larger β after oxidization due to the change of its sign for systems with donor substituent. TDDFT results show that after oxidization, the larger off-diagonal tensor β_{zxx} can be attributed to the contribution from the first excited state with the *x*-polarized CT transition. Finally, the frequency-dependent β values of the species **3** with diprotonation were calculated by coupled-perturbed DFT method, and the results exhibit a small dispersion effect at the low-frequency region and further suggest that the oxidized process can strongly influence the second-order NLO responses.

Acknowledgments

The authors gratefully acknowledge the financial support from the Natural Science Foundation of China (No. 21173035) and the Natural Science Foundation of Jilin province (20101154).

Appendix A. Supplementary data

Supplementary data associated with this article can be found, in the online version, at http://dx.doi.org/10.1016/j.jmgm.2012.07.001.

References

[1] B.J. Coe, Switchable nonlinear optical metallochromophores with pyridinium electron acceptor groups, Accounts of Chemical Research 39 (2006) 383–393.
[2] K.A. Green, M.P. Cifuentes, M. Samoc, M.G. Humphrey, Metal alkynyl complexes as switchable NLO systems, Coordination Chemistry Reviews 255 (2011) 2530–2541.
[3] K.A. Green, M.P. Cifuentes, T.C. Corkery, M. Samoc, M.G. Humphrey, Switching the cubic nonlinear optical properties of an electro-, halo-, and photochromic ruthenium alkynyl complex across six states, Angewandte Chemie International Edition 48 (2009) 7867–7870.
[4] I. Asselberghs, K. Clays, A. Persoons, M.D. Ward, J. McCleverty, Switching of molecular second-order polarisability in solution, Journal of Materials Chemistry 14 (2004) 2831–2839.
[5] I. Asselberghs, G. Hennrich, J. McCleverty, L. Boubekeur-Lecaque, B.J. Coe, K. Clays, Organic materials for molecular switching, Proceedings of the SPIE – The International Society for Optical Engineering 6999 (2008) 69991W.
[6] H.B. Zhao, Y.Q. Qiu, C.G. Liu, S.L. Sun, Y. Liu, R.S. Wang, Redox-switchable second-order nonlinear optical responses of TEMPO-dithiolate ligand and (tempodt)M complexes (M = Pt, Pd), Journal of Organometallic Chemistry 695 (2010) 2251–2257.
[7] S. Di Bella, C. Dragonetti, M. Pizzotti, D. Roberto, F. Tessore, R. Ugo, Coordination and organometallic complexes as second-order nonlinear optical molecular materials, Topics in Organometallic Chemistry 28 (2010) 1–55.
[8] A. Baccouche, B. Peigné, F. Ibersiene, D. Hammoutène, A. Boutarfaïa, A. Boucekkine, C. Feuvrie, O. Maury, I. Ledoux, H. Le Bozec, Effects of the metal center and substituting groups on the linear and nonlinear optical properties of substituted styryl-bipyridine metal(II) dichloride complexes: DFT and TDDFT computational investigations and harmonic light scattering measurements, Journal of Physical Chemistry A 114 (2010) 5429–5438.
[9] A. Valore, A. Colombo, C. Dragonetti, S. Righetto, D. Roberto, R. Ugo, F. De Angelis, S. Fantacci, Luminescent cyclometallated Ir(III) and Pt(II) complexes with β-diketonate ligands as highly active second-order NLO chromophores, Chemical Communications 46 (2010) 2414–2416.
[10] B.J. Coe, S.P. Foxon, E.C. Harper, M. Helliwell, J. Raftery, C.A. Swanson, B.S. Brunschwig, K. Clays, E. Franz, J. Garín, J. Orduna, P.N. Horton, M.B. Hursthouse, Evolution of linear absorption and nonlinear optical properties in v-shaped ruthenium(II)-based chromophores, Journal of the American Chemical Society 132 (2010) 1706–1723.
[11] B.J. Coe, J. Fielden, S.P. Foxon, I. Asselberghs, K. Clays, B.S. Brunschwig, Two-dimensional, pyrazine-based nonlinear optical chromophores with ruthenium(II) ammine electron donors, Inorganic Chemistry 49 (2010) 10718–10726.
[12] O. Maury, H. Le Bozec, Molecular engineering of octupolar NLO molecules and materials based on bipyridyl metal complexes, Accounts of Chemical Research 38 (2005) 691–704.
[13] N.N. Ma, G.C. Yang, S.L. Sun, C.G. Liu, Y.Q. Qiu, Computational study on second-order nonlinear optical (NLO) properties of a novel class of two-dimensional Λ- and W-shaped sandwich metallocarborane-containing chromophores, Journal of Organometallic Chemistry 696 (2011) 2380–2387.
[14] S. Di Bella, I. Fragalà, Two-dimensional characteristics of the second-order nonlinear optical response in dipolar donor–acceptor coordination complexes, New Journal of Chemistry 26 (2002) 285–290.
[15] C.G. Liu, X.H. Guan, Z.M. Su, Computational study on redox-switchable 2D second-order nonlinear optical properties of push–pull monotetrathiafulvalene–bis (salicylaldiminato) Zn(II) Schiff base complexes, Journal of Physical Chemistry C 115 (2011) 6024–6032.
[16] W. Zhang, W.H. Sun, S. Zhang, J. Hou, K. Wedeking, S. Schultz, R. Fröhlich, H. Song, Synthesis, characterization, and ethylene oligomerization and polymerization of [2,6-bis(2-benzimidazolyl)pyridyl]chromium chlorides, Organometallics 25 (2006) 1961–1969.
[17] T. Ayers, N. Caylor, G. Ayers, C. Godwin, D.J. Hathcock, V. Stuman, S.J. Slattery, Design and investigation of a Ru(II) *N*-heterocyclic complex which undergoes proton coupled electron transfer, Inorganica Chimica Acta 328 (2002) 33–38.
[18] H. Yang, W.T. Chen, D.F. Qiu, X.Y. Bao, W.R. Xing, S.S. Liu, Synthesis, characterization and DNA-binding studies of new tridentate polypyridyl cobalt(II) and ruthenium(II) complexes, Acta Chimica Sinica 24 (2007) 2959–2964 (in Chinese).
[19] B. Schulze, D. Escudero, C. Friebe, R. Siebert, H. Görls, U. Köhn, E. Altuntas, A. Baumgaertel, M.D. Hager, A. Winter, B. Dietzek, J. Popp, L. González, U.S. Schubert, A heteroleptic bis(tridentate) ruthenium(II) complex of a click-derived abnormal carbene pincer ligand with potential for photosensitzer application, Chemistry: A European Journal 17 (2011) 5494–5498.
[20] M.A. Haga, T. Takasugi, A. Tomie, M. Ishizuya, T. Yamada, M. Delower Hossain, M. Inoue, Molecular design of a proton-induced molecular switch based on rod-shaped Ru dinuclear complexes with bis-tridentate 2,6-bis(benzimidazol-2-yl)pyridine derivatives, Dalton Transactions (2003) 2069–2079.
[21] D. Mishra, A. Barbieri, C. Sabatini, M.G.B. Drew, H.M. Figgie, W.S. Sheldrick, S.K. Chattopadhyay, Tuning of redox potential and visible absorption band of ruthenium(II) complexes of (benzimidazolyl) derivatives: synthesis, characterization, spectroscopic and redox properties, X-ray structures and DFT calculations, Inorganica Chimica Acta 360 (2007) 2231–2244.
[22] A. Singh, B. Chetia, S.M. Mobin, G. Das, P.K. Iyer, B. Mondal, Ruthenium monoterpyridine complexes with 2,6-bis(benzimidazol-2-yl)pyridine: synthesis, spectral properties and structure, Polyhedron 27 (2008) 1983–1988.
[23] C. Bhaumik, S. Das, D. Saha, S. Dutta, S. Baitalik, Synthesis, characterization, photophysical, and anion-binding studies of luminescent heteroleptic bis-tridentate ruthenium(II) complexes based on 2,6-bis(benzimidazole-2-yl)pyridine and 4′-substituted 2,2′:6′,2″ terpyridine derivatives, Inorganic Chemistry 49 (2010) 5049–5062.
[24] X.X. Sun, G.C. Yang, S.L. Sun, N.N. Ma, Y.Q. Qiu, Effects of the substituting groups and proton abstraction on the nonlinear optical properties of heteroleptic bis-tridentate Ru(II) complexes, Journal of Organometallic Chemistry 696 (2011) 3384–3391.
[25] J.O. Jeppesen, J. Becher, Pyrrolo-tetrathiafulvalenes and their applications in molecular and supramolecular chemistry, European Journal of Organic Chemistry (2003) 3245–3266.
[26] C.G. Liu, W. Guan, P. Song, L.K. Yan, Z.M. Su, Redox-switchable second-order nonlinear optical responses of push–pull monotetrathiafulvalene–metalloporphyrins, Inorganic Chemistry 48 (2009) 6548–6554.
[27] J.F. Lamère, I. Malfant, A. Sournia-Saquet, P.G. Lacroix, J.M. Fabre, L. Kaboub, T. Abbaz, A.-K. Gouasmia, I. Asselberghs, K. Clays, Quadratic nonlinear optical response in partially charged donor-substituted tetrathiafulvalene: from a computational investigation to a rational synthetic feasibility, Chemistry of Materials 19 (2007) 805–815.
[28] J.Y. Balandier, M. Chas, P.I. Dron, S. Goeb, D. Canevet, A. Belyasmine, M. Allain, M. Sallé, *N*-aryl pyrrolo-tetrathiafulvalene based ligands: synthesis and metal coordination, Journal of Organic Chemistry 75 (2010) 1589–1599.
[29] J.O. Jeppesen, K. Takimiya, F. Jensen, J. Becher, Pyrrolo annelated tetrathiafulvalenes: the parent systems, Organic Letters 1 (1999) 1291–1294.
[30] M.J. Frisch, G.W. Trucks, H.B. Schlegel, G.E. Scuseria, M.A. Robb, J.R. Cheeseman, G. Scalmani, V. Barone, B. Mennucci, G.A. Petersson, H. Nakatsuji, M. Caricato, X. Li, H.P. Hratchian, A.F. Izmaylov, J. Bloino, G. Zheng, J.L. Sonnenberg, M. Hada, M. Ehara, K. Toyota, R. Fukuda, J. Hasegawa, M. Ishida, T. Nakajima, Y. Honda, O. Kitao, H. Nakai, T. Vreven, J.A. Montgomery Jr., J.E. Peralta, F. Ogliaro, M. Bearpark, J.J. Heyd, E. Brothers, K.N. Kudin, V.N. Staroverov, R. Kobayashi, J. Normand, K. Raghavachari, A. Rendell, J.C. Burant, S.S. Iyengar, J.

Tomasi, M. Cossi, N. Rega, J.M. Millam, M. Klene, J.E. Knox, J.B. Cross, V. Bakken, C. Adamo, J. Jaramillo, R. Gomperts, R.E. Stratmann, O. Yazyev, A.J. Austin, R. Cammi, C. Pomelli, J.W. Ochterski, R.L. Martin, K. Morokuma, V.G. Zakrzewski, G.A. Voth, P. Salvador, J.J. Dannenberg, S. Dapprich, A.D. Daniels, O. Farkas, J.B. Foresman, J.V. Ortiz, J. Cioslowski, D.J. Fox, Gaussian 09 Revision A. 02, Gaussian, Inc., Wallingford, CT, 2009.

[31] D.R. Kanis, M.A. Ratner, T.J. Marks, Design and construction of molecular assemblies with large second-order optical nonlinearities. Quantum chemical aspects, Chemical Reviews 94 (1994) 195–242.
[32] S.I. Gorelsky, *AOMix* Manual (www.sg-chem.net).
[33] Y.Z. Lan, W.D. Cheng, D.S. Wu, J. Shen, S.P. Huang, H. Zhang, Y.J. Gong, F.F. Li, A theoretical investigation of hyperpolarizability for small Ga_nAs_m ($n+m=4$–10) clusters, Journal of Chemical Physics 124 (2006) 094302.